PERGAMON

International Journal of Heat and Mass Transfer 41 (1998) 4167–4182

International Journal of HEAT and MASS TRANSFER

Thermophoretic deposition of small particles in a direct numerical simulation of turbulent channel flow

D. G. Thakurta[a], M. Chen[a], J. B. McLaughlin[a,*], K. Kontomaris[b]

[a] *Department of Chemical Engineering, Clarkson University, Potsdam, NY 13699-5705, U.S.A.*
[b] *DuPont Central Research and Development, Experimental Station, Wilmington, DE 19880-0304, U.S.A.*

Received 30 September 1997; in final form 24 March 1998

Abstract

This paper presents results for the deposition rate of small particles on the walls of a turbulent channel flow. The results were obtained by direct numerical simulation of a horizontal turbulent channel flow. A temperature profile typical of ceramic oxide aerosol reactors was imposed across the channel. Thermophoresis played an important role in the deposition of particles for the range of conditions that were studied. An interaction between turbophoresis and thermophoresis was found to play an important role in the deposition process. © 1998 Elsevier Science Ltd. All rights reserved.

Nomenclature

a particle radius
a_p particle acceleration
C particle concentration
C_b particle bulk concentration
C_c Cunningham slip factor
C_D nonlinear correction to Stokes drag
d particle diameter
$\mathbf{F}_b$ Brownian random force
$\mathbf{F}_d$ wall-corrected Stokes drag force
$\mathbf{F}_l$ lift force
$\mathbf{F}_T$ thermophoretic force
$\mathbf{g}$ gravitational acceleration
h channel half width
j_d flux of depositing particles
k_g, k_p thermal conductivity of fluid and particle, respectively
k_T thermal slip coefficient
K thermophoretic coefficient
N_d total number of particles deposited on the channel walls
N_{bot} number of particles deposited on the bottom channel wall
N_{top} number of particles deposited on the top channel wall
N_x, N_y, N_z number of grid points in the downstream, normal and spanwise directions, respectively
p pressure
p' pressure fluctuations
Pr Prandtl number
Re Reynolds number of channel flow based on hydraulic diameter and bulk velocity
S particle–fluid density ratio
Sc particle Schmidt number
t time
T mean fluid temperature
T_c mean fluid temperature at core
T_w mean fluid temperature at wall
T_* friction temperature
u_* friction velocity
u, v, w fluid fluctuation velocities in downstream, normal and spanwise directions, respectively
u', v', w' fluid rms fluctuations in downstream, normal and spanwise directions, respectively
U mean downstream component of fluid velocity
$\mathbf{v}$ fluid velocity
v_{imp} normal component of impact velocity of depositing particles
$\mathbf{v}_p$ particle velocity
V_d deposition velocity
x coordinate in downstream direction

* Corresponding author. Tel.: +001-315-268-6663; Fax: +001-315-268-6654; E-mail: jmclau@sun.soe.clarkson.edu

PII: S0017-9310(98)00135-5

$\hat{\mathbf{x}}, \hat{\mathbf{y}}, \hat{\mathbf{z}}$ unit vectors in the streamwise, normal and spanwise direction, respectively
y coordinate measured from nearest wall in normal direction
z coordinate in spanwise direction.

Greek symbols
α thermal diffusivity
θ temperature fluctuations
λ molecular mean free path in the fluid
λ_x, λ_z period in the streamwise and spanwise direction, respectively
μ fluid dynamic viscosity
ρ fluid density
ρ_p particle density
τ particle relaxation time.

Subscript
p of particle
T due to thermophoresis
w quantity at wall
x, y, z streamwise, normal and spanwise component.

Superscript
$+$ nondimensional quantity in wall variable.

Miscellaneous
$\langle\ \rangle$ xz-plane space averaged quantities
$\bar{\ }$ time averaged quantities
$|\ |$ absolute values.

1. Introduction

The goal of this work was to gain a better understanding of the deposition of titania (TiO_2) particles, sized 0.05 μm through 1.66 μm, in a turbulent channel flow with an imposed mean temperature gradient. A direct numerical simulation (DNS) of a turbulent channel flow ($Re = 7050$) was used to study deposition of these particles on the walls of the channel. In performing the computations of particle deposition, material property variations were ignored.

This study was motivated by a desire to better understand the role of thermophoresis in ceramic oxide aerosol reactors. The reactions in question are highly exothermic so that the core of the reactor tube is hotter than the wall. When a temperature gradient is established in a gas, the aerosol particles in the gas experience a force in the direction of decreasing temperature. The motion of the aerosol particles that results from this force is called thermophoresis. The magnitude of the thermal force depends on gas and particle properties and on the temperature gradient. When cold surfaces are near a hot gas, thermophoresis can cause particles in the gas to be deposited on the cold surfaces. According to Xiong and Pratsinis [1], as many as 50% of the particles in a commercial ceramic oxide reactor can be brought to the reactor walls by thermophoresis.

Derjaguin et al. [2] performed experiments on thermophoretic migration in gases and used their results to determine the constants in an expression for the thermophoretic constant. Walker et al. [3] used the above results to compute the thermophoretic velocity in a study of thermophoretic deposition in laminar pipe flow.

Fernandez de la Mora and Rosner [4] and Gökoğlu and Rosner [5] performed analyses for thermophoretic deposition on solid surfaces. Fernandez de la Mora and Rosner used asymptotic analysis to derive results for the deposition of particles on spheres and cylinders at small Reynolds numbers. Gökoğlu and Rosner developed correlations for deposition of small particles on solid surfaces from boundary layers at large Reynolds numbers. They discussed turbulent boundary layers as well as laminar boundary layers.

Although one of the correlations developed by Gökoğlu and Rosner is for turbulent boundary layers, it is not appropriate for the conditions that will be considered in this paper. Gökoğlu and Rosner assumed that particles are brought close to the wall by turbulent diffusion and then deposit by thermophoresis (or other effects that they considered). However, when particle inertia is an important effect, Caporaloni et al. [6] and, independently, Reeks [7] showed that 'turbophoresis' can cause particles to migrate toward a wall from a turbulent shear flow. Turbophoresis causes particle to migrate, in a average sense, from regions of large rms turbulent velocity fluctuations to regions of small rms turbulent velocity fluctuations.

McLaughlin [8] used DNS to study aerosol deposition in an isotherml turbulent channel flow. Although the particles were much larger than those to be discussed in this paper, the channel flow was vertical so that gravity could not directly cause the deposition of particles on the channel walls. It was found that particles tended to accumulated in the viscous wall region by turbophoresis. It was also found that a large fraction of the particles that deposited travelled to the wall by a 'free-flight' mechanism similar in spirit to that suggested by Friedlander and Johnstone [9]. Brooke et al. [10, 11] and Chen et al. [12] further documented the phenomena of free-flight and the tendency of aerosols to accumulate near walls in turbulent flows.

The particles that will be discussed in this paper are in the size range 0.05–1.66 μm. Under many circumstances, one would expect the correlation developed by Gökoğlu and Rosner to provide useful estimates of the thermophoretic deposition rates. However, the friction velocities in aerosol reactors are large enough that particle inertia plays an important role in their behavior near walls. It will be seen that turbophoresis plays an important role in the deposition process. For example the concentration

profile shows a maximum near the wall so that the concentration profile has the 'wrong' slope for a model based on turbulent diffusion to be appropriate.

2. Simulation procedures for flow and temperature fields

2.1. Flow geometry

The channel flow program solves the incompressible Navier–Stokes equation for a turbulent pressure driven flow between two infinite, flat, parallel walls. The x-direction points downstream in the direction of the constant mean pressure gradient parallel to the walls, the y-direction is normal to the walls and the z-direction points in the spanwise direction parallel to the walls. A mean velocity is present only in the x-direction and is denoted by U. The fluctuations of the x-, y- and z-components of the velocity are denoted by u, v and w, respectively. Hence, the components of the fluid velocity in the x-, y-, and z-directions are given by $U+u$, v and w, respectively. The computation domain is periodic in the streamwise and spanwise directions with corresponding periods λ_x and λ_z. It is valid to impose periodic conditions in the x- and z-directions since the fluid is unbounded in those directions. Ideally, λ_x and λ_z should be much larger than the distance between the channel walls, $2h$.

2.2. Simulation of flow field

In the calculations of thermophoresis, material property variations were ignored. Thus, the momentum equation takes the form of the Navier–Stokes equation for an incompressible fluid with no body forces:

$$\rho\frac{\partial \mathbf{v}}{\partial t}+\rho\mathbf{v}\cdot\nabla\mathbf{v}=-\nabla p+\mu\nabla^2\mathbf{v}. \tag{1}$$

In the above equation, $\mathbf{v}=(U+u)\hat{\mathbf{x}}+v\hat{\mathbf{y}}+w\hat{\mathbf{z}}$ is the fluid velocity field ($\hat{\mathbf{x}}$, $\hat{\mathbf{y}}$ and $\hat{\mathbf{z}}$ are unit vectors in the x-, y- and the z-direction, respectively), p is the pressure, t is the time, and ρ and μ are the fluid density and fluid dynamic viscosity, respectively.

The fluid is assumed to be incompressible and to satisfy rigid, no-slip boundary conditions on the channel walls

$$\nabla\cdot\mathbf{v}=0 \tag{2}$$

$$\mathbf{v}=0,\quad y=\pm h. \tag{3}$$

In addition, periodic boundary conditions are imposed in the downstream and spanwise directions

$$\mathbf{v}(x+m\lambda_x,y,z+n\lambda_z,t)=\mathbf{v}(x,y,z,t). \tag{4}$$

In the above equation m and n are integers. The periods λ_x and λ_z are chosen large enough that all important length scales are resolved. Since periodic boundary conditions are used in the x- and z-directions, the velocity, pressure head and temperature fields are expanded in terms of Fourier series in those directions. Due to the presence of rigid walls in the y-direction, the velocity, pressure head and temperature fields are expanded in terms of Chebyshev polynomial series in that direction.

In what follows, variables will be expressed in terms of 'wall units' based on ρ, μ, and the friction velocity u_*. Dimensionless quantities will be denoted by a '+' superscript. The velocity scale, length scale and time scale are u_*, $\mu/\rho u_*$ and $\mu/\rho u^2{}_*$, respectively.

2.3. Simulation of temperature field

The mean temperature profile is calculated from the wall temperature, T_w, and the mean temperature at the center of the channel, T_c using an empirical correlation. In some of the computations to be reported, temperature fluctuations were ignored in computing the thermophoretic and Brownian forces. In other computations, the above profile was imposed on the horizontally averaged temperature field and the temperature fluctuations were computed. In the latter case, the total temperature is given by $T+\theta$, where T is the time averaged temperature profile and θ is the temperature fluctuation.

For a thermally developed flow, the time averaged temperature profile, T, is a function only of y. It is calculated by using an empirical 'law of the wall temperature profile' given by Deissler (Bird et al. [13]), which is presented below. For a region near the wall ($y^+<26$)

$$T^+=\int_0^{y^+}\frac{\mathrm{d}y^+}{(1/Pr)+n^2U^+y^+(1-\exp\{-n^2U^+y^+\})}+T_w^+, \tag{5}$$

and for the turbulent core ($y^+\geqslant 26$)

$$T^+=U^+-U^+(y^+=26)+T^+(y^+=26). \tag{6}$$

In the above equations y^+ is the distance measured from the closest channel wall, Pr is the Prandtl number of the fluid, and n is a constant ($=0.124$). The symbols T^+ and T_w^+ denote the dimensionless time averaged temperatures at y^+ and at the walls, respectively. Temperatures are non-dimensionalized with T_*:

$$T_*=\frac{1}{Pr}\frac{\mu}{\rho u_*}\left|\frac{\mathrm{d}T}{\mathrm{d}y}\right|_{\text{wall}}=\frac{1}{Pr}\left|\frac{\mathrm{d}T}{\mathrm{d}y^+}\right|_{\text{wall}}. \tag{7}$$

In equations (5) and (6), an empirical fit is used to calculate $U^+(y^+)$.

$$U^+(y^+)=16\left(1-\exp\left\{\frac{y^{+2}-2y^+h^+}{32h^+}\right\}\right). \tag{8}$$

The temperature satisfies

$$\frac{\partial(T+\theta)}{\partial t}+\mathbf{v}\cdot\nabla(T+\theta)=\alpha\nabla^2(T+\theta). \tag{9}$$

The mean temperature satisfies

$$\langle\overline{\mathbf{v}\cdot\nabla\theta}\rangle = \alpha\frac{\mathrm{d}^2T}{\mathrm{d}y^2} \tag{10}$$

where α is the thermal diffusivity. The fluctuating temperature, θ, is obtained by solving the following equation:

$$\frac{\partial\theta}{\partial t}+\mathbf{v}\cdot\nabla\theta-\langle\overline{\mathbf{v}\cdot\nabla\theta}\rangle+v\frac{\mathrm{d}T}{\mathrm{d}y}=\alpha\nabla^2\theta. \tag{11}$$

Equation (11) is obtained by subtracting equation (10) from (9). The above equation may be non-dimensionalized with u_*, ρ, μ and T_*:

$$\frac{\partial\theta^+}{\partial t^+}+\mathbf{v}^+\cdot\nabla^+\theta^+-\langle\overline{\mathbf{v}^+\cdot\nabla^+\theta^+}\rangle+v^+\frac{\mathrm{d}T^+}{\mathrm{d}y^+}=\frac{1}{Pr}\nabla^{+2}\theta^+. \tag{12}$$

The fluctuating temperature satisfies periodic boundary conditions [similar to equation (4)] in the streamwise and spanwise directions and homogeneous boundary conditions at the channel walls.

$$\theta(x+m\lambda_x,y,z+n\lambda_z,t)=\theta(x,y,z,t),\qquad \theta(x,\pm h,z,t)=0. \tag{13}$$

Using equation (13) one can show that

$$\langle\overline{\mathbf{v}\cdot\nabla\theta}\rangle=\frac{\partial}{\partial y}\langle\overline{v\theta}\rangle.$$

2.4. Physical parameters of the fluid

Xiong and Pratsinis [1] discuss the production of ceramic oxide fine particles using TiO_2 as a specific example. They provide typical ranges for operating parameters and the parameters chosen for the work are in the above ranges. The temperatures are 1773 K at the core and 1523 K at the reactor walls. The physical properties of the fluid are based on the properties of chlorine gas at 1648 K, which is the average temperature based on the temperature of the core and that at the walls of the channel. All physical parameters used in the simulation are listed in Table 1. The symbol λ denotes the mean free path length in the fluid and k_g denotes the thermal conductivity of the fluid.

2.5. Simulation parameters

The computational domain used for the DNS spans 630 wall units in the spanwise and streamwise directions and 250 wall units in the normal direction. The computational domain contains $16\times65\times64$ grid points in the streamwise, the normal, and the spanwise directions, respectively. The grid spacings are given in Table 2. The time step used in this work was 0.25 time wall units.

Lyons et al. [14] generated steady-state velocity fields that were used to obtain the flow fields used in this work. Figure 1 shows the root mean square temperature and velocity fluctuations in comparison with experimental results [15, 16]. The results of Kreplin and Eckelmann [15] are for the normal component of velocity. The Reynolds number in the present simulation is 7050 based on the hydraulic diameter and the bulk velocity.

The initial velocity field was a steady-state turbulent flow field. The initial temperature field was the mean temperature profile described by equations (5) and (6). The turbulent velocity field quickly generated a turbulent temperature field. The value of T_* was computed from equation (7), in which the following value of the temperature gradient at the wall was used:

$$\left|\frac{\mathrm{d}T}{\mathrm{d}y^+}\right|_{\mathrm{wall}}\simeq\frac{T_\mathrm{c}-T_\mathrm{w}}{19.178}=13.036\,\mathrm{K/wall\ unit}. \tag{14}$$

Note that the dimensionless temperature gradient at the wall is equal to the Prandtl number, Pr.

3. Simulation of particle motion

The particle's equation of motion includes the Stokes drag force, the Brownian random force, the lift force and the thermophoretic force. With the exception of the thermophoretic force, the details may be found in Chen and McLaughlin [12]. The equation takes the following form:

$$\frac{\mathrm{d}\mathbf{v}_\mathrm{p}^+}{\mathrm{d}t^+}=\frac{2(S-1)}{2S+1}\mathbf{g}^+ + C_\mathrm{D}\mathbf{F}_\mathrm{d}^+ + \mathbf{F}_\mathrm{l}^+ + \mathbf{F}_\mathrm{b}^+ + \mathbf{F}_\mathrm{T}^+. \tag{15}$$

In equation (15) C_D is the nonlinear drag correction factor, $\mathbf{F}_\mathrm{d}^+$ is the dimensionless Stokes drag force including wall corrections and the Cunningham slip correction, $\mathbf{F}_\mathrm{l}^+$ is the dimensionless lift force, $\mathbf{F}_\mathrm{b}^+$ is the dimensionless Brownian random force, and, $\mathbf{F}_\mathrm{T}^+$ is the dimensionless thermophoretic force. With the exception of the thermophoretic force, expressions for the above various forces may be found in Chen and McLaughlin.

The Stokes drag in equation (15) may be expressed in

Table 1
Physical properties of the fluid

λ 0.115×10^{-6} m	k_g 0.0508 W ($\mathrm{m^{-1}\,K^{-1}}$)	T_w 1523 K
ρ 1.5 kg $\mathrm{m^{-3}}$	Pr 0.784	u_* 7 m $\mathrm{s^{-1}}$
μ 7.5×10^{-5} kg ($\mathrm{m^{-1}\,s^{-1}}$)	T_c 1773 K	T_* 16.627 K

Table 2
Computational grid

$\lambda_x^+=630$	$N_x=16$	$\Delta x^+=39.40$
$2\mathrm{h}^+=250$	$N_y=65$	$\Delta y^+=0.15$–6.13
$\lambda_z^+=630$	$N_z=64$	$\Delta z^+=9.84$

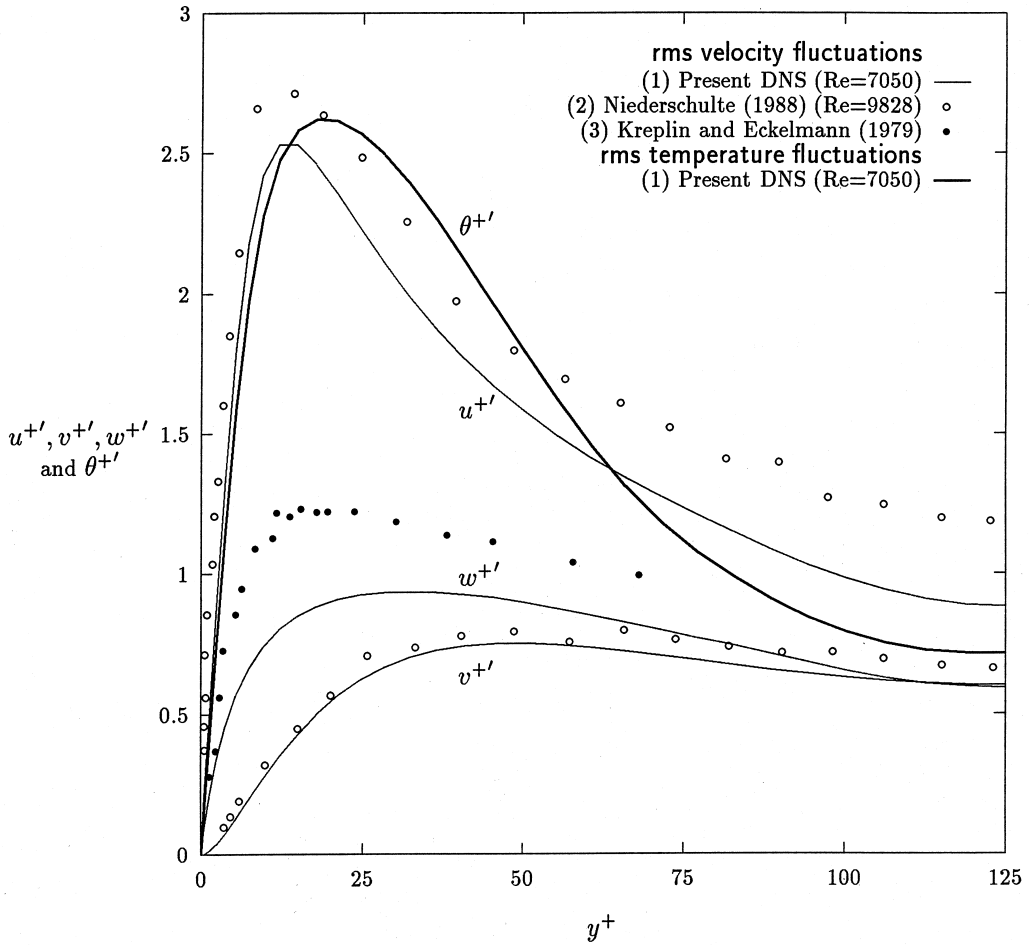

Fig. 1. Root mean square temperature and velocity fluctuations in comparison with experimental results.

terms of the dimensionless Stokes particle relaxation time, τ^+, which is defined by

$$\tau^+ = C_c \frac{2S+1}{9} a^{+2}. \tag{16}$$

The dimensionless particle relaxation time may be interpreted as a dimensionless stopping distance. If a particle were projected with an initial velocity equal to the friction velocity into a stagnant gas, τ^+ is the dimensionless stopping distance of the particle. Thus, τ^+ is a useful way of characterizing particle inertia. Particles with $\tau^+ \ll 1$ may be expected to follow turbulent eddies (provided that the sedimentation velocity, thermophoretic velocity, and Brownian motion can be neglected).

The following expression for the thermophoretic velocity, $\mathbf{v}_{pT}$, of a particle is given by Walker et al. [3].

$$\mathbf{v}_{pT} = -K\frac{v}{T}\nabla T. \tag{17}$$

Here K is the thermophoretic coefficient. Expressions for the thermophoretic coefficient for the regime where the mean free path, λ, is comparable to or larger than the particle radius, a, are given by Derjaguin et al. [2]:

$$K = k_T \frac{\left(1 + c_1 \frac{\lambda}{a}\frac{k_p}{k_g}\right)}{\left(1 + \frac{k_p}{k_g} + c_1 \frac{\lambda}{a}\frac{k_p}{k_g}\right)}, \tag{18}$$

where c_1 is a constant ($=2.17$), k_T is the thermal slip coefficient (≈ 1.1), and k_p and k_g are the thermal conductivities of the particle and the fluid, respectively.

The expression for the thermophoretic force, $\mathbf{F}_T^+$, in equation (15) can be obtained by multiplying the thermophoretic velocity [equation (17)] by the mass of the particle and dividing it by the particle relaxation time τ, and then making the obtained expression dimensionless:

$$\mathbf{F}_T^+ = -\frac{K}{\tau^+}\frac{\nabla T^+}{T^+}. \tag{19}$$

Table 3
Physical properties of the aerosol particles

d	0.05, 0.20, 0.50, 0.06, 1.00 and 1.66 μm
ρ_p	4260 kg m^{-3}
k_p	3.0 W (m^{-1} K^{-1})

Table 4
Length and time scales

u_* (m s^{-1})	Wall unit (m)	Time wall unit (s)
7	7.1429×10^{-6}	1.0204×10^{-6}
4	1.2500×10^{-5}	3.1250×10^{-6}

3.1. Physical parameters of the particles

The diameters of the titania particles in the present study ranged from 0.05–1.66 μm. Other physical properties are listed in Table 3.

3.2. Particle tracking

In the evaluation of the drag force and the lift force in the particle equation of motion, the velocity of the undisturbed fluid at the location of each particle is required. Similarly, for the computation of the thermophoretic force, the temperature and its gradient at the location of the particle are needed. Since the particles are not located at the three-dimensional grid points, an interpolation scheme is required. In this work, partial Hermite interpolation was used to obtain the fluid velocity, the temperature and its gradient at a particle location. Partial Hermite interpolation gives reasonable accuracy and saves computation time (see Kontomaris et al. [17]). A second-order time stepping method was used to compute the trajectories of the particles by solving equation (15) and

$$\frac{\mathrm{d}x^+}{\mathrm{d}t^+} = \mathbf{v}_p^+ \tag{20}$$

simultaneously with the DNS. On the first time step, an Euler method was used.

4. Results

4.1. Thermophoretic deposition in a stagnant gas

For the purpose of comparison with the DNS results, the rate of deposition and impact velocities for particles dispersed in a stagnant gas were computed. The thermophoretic force, $\mathbf{F}_T^+$, on an aerosol particle was calculated based on equation (19). Only the mean temperature profile was used in the computations. Table 4 shows the values of the length and time scales for two different values of friction velocity u_* used subsequently. For the analysis in stagnant gas, the value of u_* was 7 m s^{-1}. Physical properties of the fluid and the particles are listed in Tables 1 and 3, respectively. Table 5 shows the various parameters for solid particles used in the runs. In Table 5, d is the particle diameter, C_c is the Cunningham slip correction factor, and Sc is the particle Schmidt number.

Since the temperature gradient exists only in the normal direction, F_{Ty}^+ is the only non-zero component of the thermophoretic force. The magnitude of the thermophoretic velocity at the wall for different particle sizes was computed from equation (17). Equation (17) is nondimensionalized, and with the help of equation (14) it can be simplified to the following form:

$$v_{pT_y}^+|_{\mathrm{wall}} = -K\frac{1}{T^+}\frac{\mathrm{d}T^+}{\mathrm{d}y^+}\bigg|_{\mathrm{wall}} = -K\frac{1}{1523}\times 13.036. \tag{21}$$

The values of K can be calculated from equation (18).

Table 5
Parameters for the solid particles

u_* (m s^{-1})	d (μm)	d^+	C_c	Sc	τ (s)	τ^+
7	0.05	0.007	8.231	9.438×10^{3}	6.494×10^{-8}	0.064
7	0.20	0.028	2.622	1.185×10^{3}	3.311×10^{-7}	0.324
7	0.50	0.070	1.595	4.870×10^{5}	1.259×10^{-6}	1.233
7	0.60	0.084	1.491	6.254×10^{5}	1.694×10^{-6}	1.660
7	1.00	0.140	1.290	1.205×10^{6}	4.071×10^{-6}	3.990
7	1.66	0.232	1.174	2.196×10^{6}	10.180×10^{-5}	9.976
4	0.20	0.016	2.622	1.185×10^{5}	3.311×10^{-7}	0.106
4	0.50	0.040	1.595	4.870×10^{5}	1.259×10^{-6}	0.403
4	1.00	0.080	1.290	1.205×10^{6}	4.071×10^{-6}	1.303

Table 6
Thermophoretic velocity of particle at the wall

d (μm)	τ^+	K	$\lvert v^+_{imp}\rvert \simeq \lvert v^+_{pT_y}\rvert_{wall}$	$\log_{10}\lvert v^+_{imp}\rvert$
0.05	0.064	1.000	8.559×10^{-3}	−2.068
0.20	0.324	0.787	6.736×10^{-3}	−2.172
0.50	1.233	0.554	4.742×10^{-3}	−2.324
0.60	1.660	0.505	4.322×10^{-3}	−2.364
1.00	3.990	0.374	3.201×10^{-3}	−2.495
1.66	9.976	0.265	2.268×10^{-3}	−2.644

These have been tabulated in Table 6 together with the thermophoretic velocity at the wall. Figure 2 shows the magnitude of the thermophoretic velocity of a particle at the wall for different particle relaxation times. This velocity is a very good approximation to the impact velocity, v^+_{imp}, of the depositing particles. Table 6 also shows $\log_{10}|v^+_{imp}|$, which will be useful later for comparison purposes.

A numerical experiment was devised to estimate the deposition rate of the TiO_2 particles in a stagnant gas. Initially, 30 000 particles were uniformly distributed in the region between the two walls of the channel. These particles were then allowed to migrate and deposit on the walls due to thermophoresis. This simulation was performed for 1000 time wall units with a time step equal to 0.25 time wall units. The particles were assumed to move with their thermophoretic velocity, as justified earlier. At each time step, the locations of the undeposited particles were updated and the new particle locations were checked for deposition. The results are tabulated in Tables 7 and 8. The symbol N_d denotes the total number of particles deposited on the walls after the complete run. The dimensionless deposition velocity, V^+_d, is a measure of the flux of particles, j_d, depositing on the walls. The quantity j_d is defined as the number of particles depositing

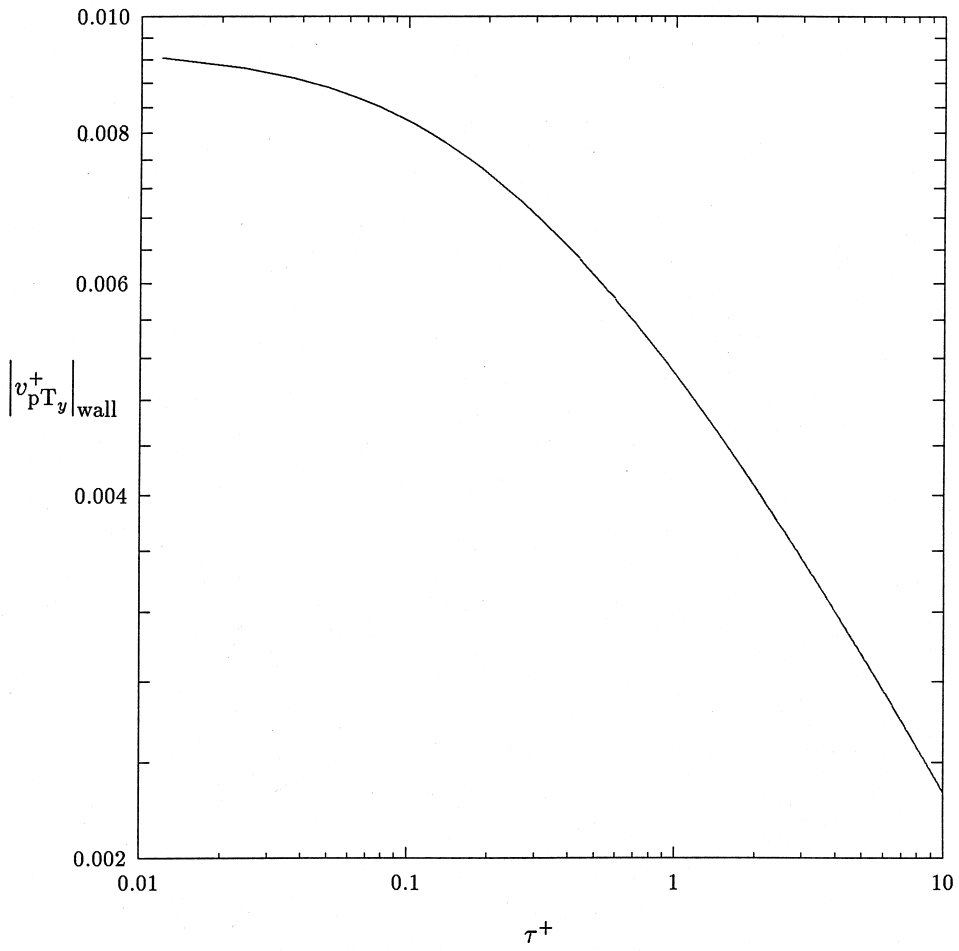

Fig. 2. Magnitude of the impact velocity for thermophoretic deposition in a stagnant gas for different particle sizes.

Table 7
Results for thermophoretic deposition in stagnant gas

No.	d (μm)	τ^+	N_d	$V_d^+ \times 10^3$
1	0.05	0.064	1861	7.886
2	0.20	0.324	1519	6.415
3	0.60	1.660	1011	4.248
4	1.00	3.990	757	3.175
5	1.66	9.976	539	2.256

Table 8
Number of particles deposited at different time intervals for thermophoretic deposition in stagnant gas

No.	t^+: 1–250	t^+: 251–500	t^+: 501–750	t^+: 751–1000	N_d
1	509	492	456	404	1861
2	401	394	376	348	1519
3	259	254	252	246	1011
4	191	192	188	186	757
5	135	136	134	134	539

Table 9
DNS run conditions

Run 1	$u_* = 7$ m s^{-1} no thermophoresis, constant temperature 1473 K
Run 2	$u_* = 7$ m s^{-1} no thermophoresis, constant temperature 1648 K
Runs 3–8	$u_* = 7$ m s^{-1} with thermophoresis, no temperature fluctuations
Runs 9–11	$u_* = 4$ m s^{-1} with thermophoresis, no temperature fluctuations
Runs 12 and 13	$u_* = 7$ m s^{-1} with thermophoresis, with temperature fluctuations

Table 10
DNS results

Run no.	d (μm)	τ^+	N_{top}	N_{bot}	$V_d^+ \times 10^3$
1	0.05	0.064	37	40	0.321
2	0.05	0.064	36	44	0.339
3	0.05	0.064	1101	1110	9.988
4	0.20	0.324	1122	1111	10.318
5	0.50	1.233	1255	1327	12.251
6	0.60	1.660	1296	1467	13.258
7	1.00	3.990	2118	2489	26.770
8	1.66	9.976	4394	4880	74.320
9	0.20	0.106	1036	1005	8.979
10	0.50	0.403	916	937	8.361
11	1.00	1.303	1001	1057	9.690
12	0.05	0.064	1103	1124	10.142
13	1.00	3.990	2118	2474	26.667

on a unit area of the wall per unit time. The symbol V_d^+ is defined as follows:

$$V_d^+ = \frac{j_d}{C_b u_*} \tag{22}$$

where C_b is the bulk concentration. The bulk concentration is calculated based on the particle concentrations between the regions $40 \leqslant y^+ \leqslant 80$ on both sides of the channel. The deposition rate decreases as the size of the particle increases due to the corresponding decrease in the magnitude of the thermophoretic force.

4.2. Thermophoretic deposition in a turbulent gas

Initially, 30 000 particles were randomly released in the numerical channel and were tracked under the effect of various forces described in Section 3. Thirteen DNS runs were performed to determine the effect of certain parameters such as the particle diameter. Each run was made for 1000 time wall units. The time step was 0.25 wall unit. Each complete run used about 32 CPU h of SGI supercomputer time at NCSA. Table 9 summarizes the conditions used in these runs. Runs 1 and 2 were carried out at constant temperature using a small particle size of 0.05 μm to check the effect of temperature on deposition by diffusion. All other runs included the thermophoretic force in the particle equation of motion. Runs 3–8 were carried out with $u_* = 7\,\mathrm{m\,s^{-1}}$. Runs 9–11 were carried out for $u_* = 4\,\mathrm{m\,s^{-1}}$. Temperature fluctuations were included for the last two runs (12 and 13).

Table 10 presents the results of all the DNS runs performed. The symbols N_{top} and N_{bot} denote the number of particles deposited on the top and the bottom wall, respectively. Table 11 shows the number of particles deposited at different time intervals. Comparison of these

Table 11
Deposition at different time intervals for the DNS runs

Run No.	t^+: 1–250	t^+: 251–500	t^+: 501–750	t^+: 751–1000	N_d
1	40	12	10	15	77
2	41	15	11	13	80
3	502	588	567	554	2211
4	447	578	625	583	2233
5	354	652	801	775	2582
6	343	731	845	844	2763
7	419	1142	1520	1526	4607
8	1231	2326	3173	2544	9274
9	443	533	562	503	2041
10	339	485	528	501	1853
11	248	481	628	701	2058
12	500	599	552	576	2227
13	424	1130	1527	1511	4592

numbers gives an idea whether the deposition process has reached a steady state.

Since the channel is horizontal, one might expect more deposition on the lower wall. However, with the exception of the largest particles, gravity has a negligible effect on the deposition of the particles. This is because of the large friction velocity used in the present simulations.

Runs 1 and 2 were performed to check the effect of temperature on the Brownian diffusivity. Particles of size 0.05 μm were chosen for this run as they primarily deposit by diffusion. No temperature gradient was imposed, and hence there was no thermophoretic effect. Run 2 was carried out at 1648 K and run 1 at 1473 K. The deposition rate was approximately 6% higher in the second run than in the first run. As one might expect, the rate of deposition due to Brownian diffusion increases with temperature. However, the increase is small.

The thermophoretic force was included in runs 3–13. Runs 3–11 only included an imposed mean temperature profile with no fluctuations. Figure 3 compares the deposition rates for thermophoretic deposition in stagnant gas (described in the previous sub-section) with the DNS results (with and without thermophoresis) for $u_* = 7\,\mathrm{m\,s^{-1}}$. DNS runs for TiO_2 particles, using the same channel dimensions and flow field, without thermophoresis were also performed for comparison purposes.

The DNS runs without thermophoresis showed that Brownian diffusion is dominant for particles with $\tau^+ < 1$ and V_d^+ can be correlated with Sc. When inertial deposition is dominant ($\tau^+ > 1$), V_d^+ in mainly determined by τ^+.

In a stagnant gas, the deposition rate due to thermophoresis decreases with increases in particle size. This is due to the decrease in the magnitude of thermophoretic force as the particle diameter increases. The value of V_d^+ for thermophoretic deposition in stagnant gas is close to V_d^+ for the DNS runs with thermophoresis for $\tau^+ < 0.1$. The thermophoretic force produces the largest increase in the deposition rate for $\tau^+ \approx 1.7$.

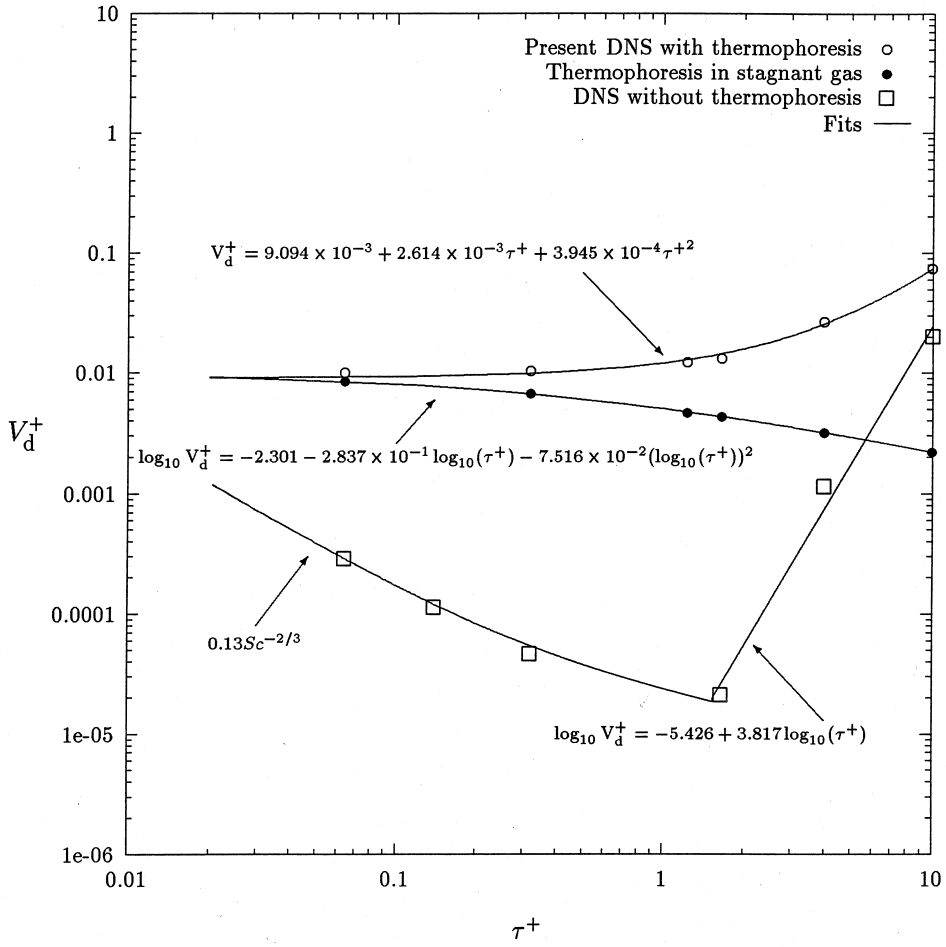

Fig. 3. Comparison of deposition rates in stagnant gas and DNS with and without thermophoresis ($u^* = 7$ m s^{-1}, runs 3–8).

Figure 4 shows the normalized concentration profiles for three different particle relaxation times after 1000 time wall units. The concentration was normalized using the bulk concentration. Smaller particles ($\tau^+ < 1$) do not show as much accumulation near the wall as bigger particles (for example $\tau^+ = 3.990$). Figure 5 compares the concentration profiles for $\tau^+ = 3.990$ for DNS runs with and without thermophoresis after a time of 1000 time wall units. The DNS run without thermophoresis shows a high concentration in the region $0.1 < y^+ < 1$. McLaughlin [8] and Brooke et al. [10] also found that aerosols tend to accumulate in this viscous wall region as a result of inertia. This phenomenon has been referred to as 'turbophoresis' by Caporaloni et al. [6] and Reeks [7]. Particles with $\tau^+ > 1$ deposit mainly by inertial motion in the absence of thermophoresis. However, some particles may not have enough inertia to penetrate the viscous wall region. They are trapped in the viscous wall region because of the relatively low turbulence level in this region. Hence, a large peak in concentration is observed in Fig. 5 for the DNS run without thermophoresis. However, when the thermophoretic force is turned on, it helps the accumulated particles in the viscous wall region to deposit by thermophoresis. The normalized concentration approximately halves for the DNS run with thermophoresis compared to the DNS run without thermophoresis.

The impact velocity spectrum reveals the dominant deposition mechanisms. Figure 6 shows plots for the number fraction of particles which deposited with a certain range of impact velocity for the DNS runs with thermophoresis against $\log_{10}|v^+_{\mathrm{imp}}|$. The solid lines represent the data for runs with thermophoresis. The impact velocity spectrum for particles with $\tau^+ = 0.064$ shows a peak at $\log_{10}|v^+_{\mathrm{imp}}| = -2.0$ that is close to the corresponding value -2.068 (see Table 6) computed earlier

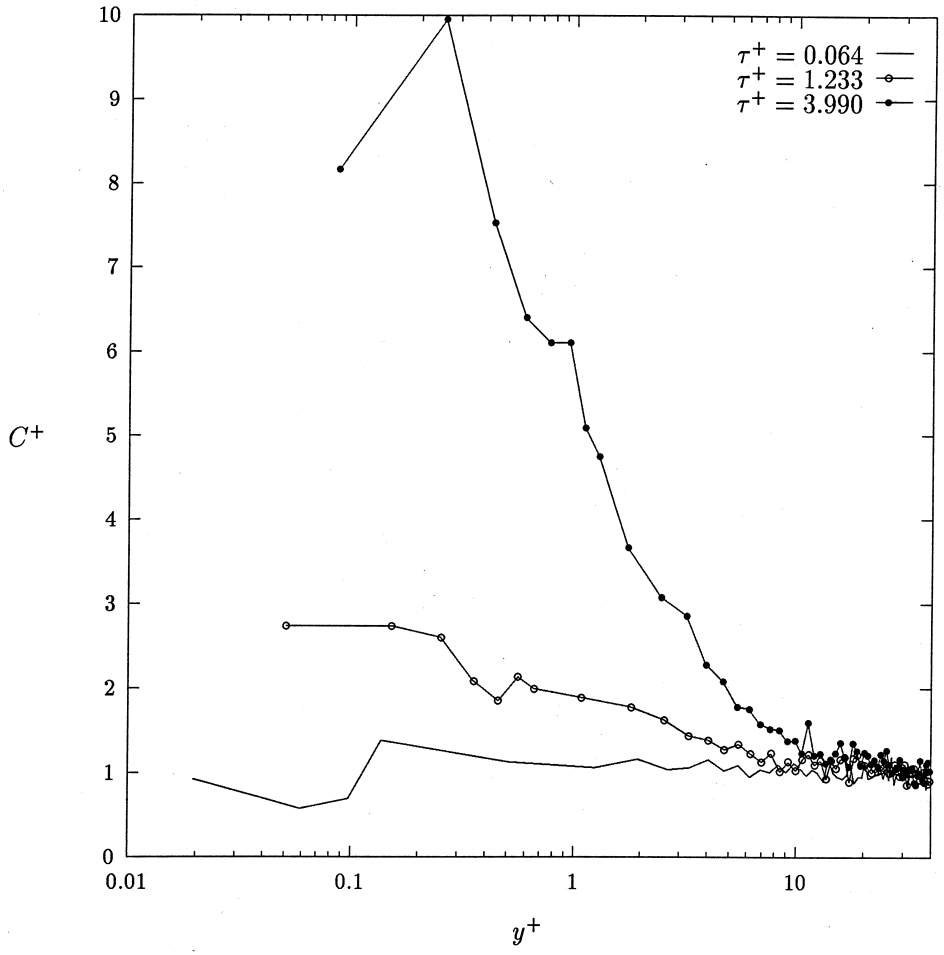

Fig. 4. Normalized concentration distribution for different size particles at $t^+ = 1000$ ($u^* = 7$ m s^{-1}, runs 3, 5 and 7).

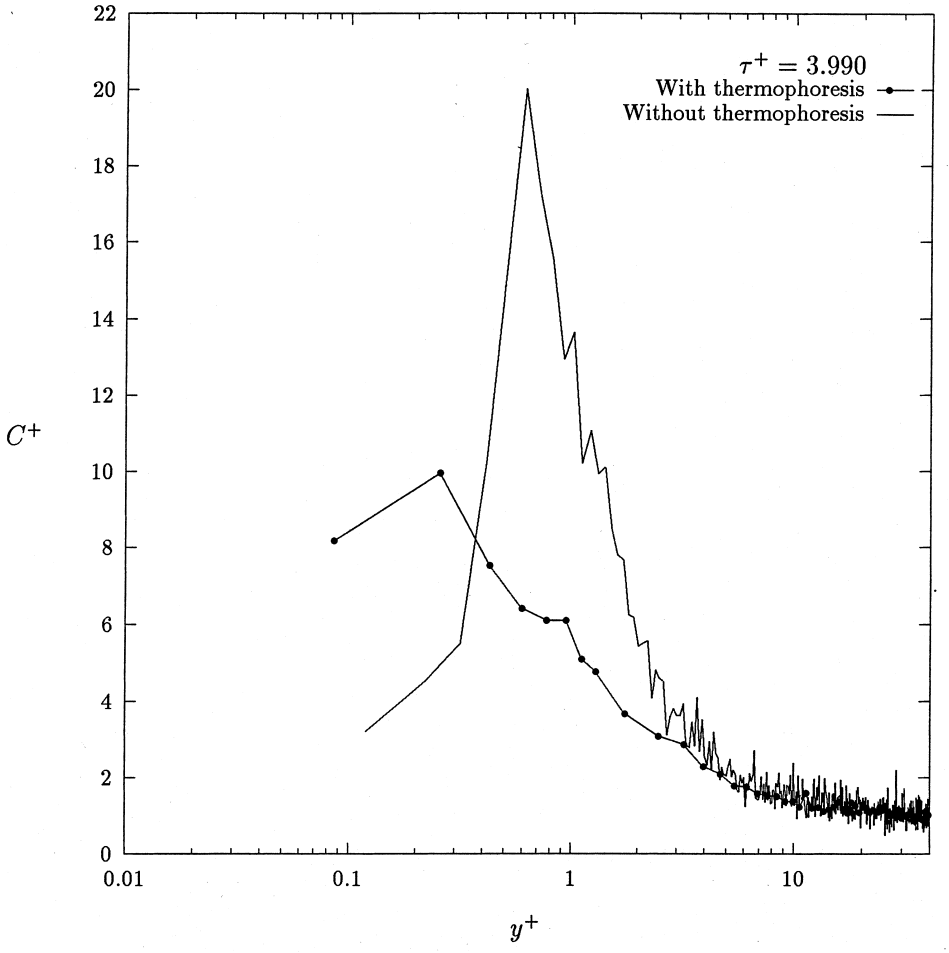

Fig. 5. Normalized concentration distribution for $\tau^+ = 3.990$ with and without thermophoresis at $t^+ = 1000$.

for thermophoretic deposition in stagnant gas. About 60% are deposited at this impact velocity which represents thermophoretic deposition. The fact that a significant number of particles deposit with significantly smaller impact velocities suggests that Brownian motion plays a role in deposition. For $\tau^+ = 1.233$ and 3.990, more than 90% of the particles are deposited due to thermophoresis as is represented by the distinct high peaks. These peaks move to the left as τ^+ increases. This is because larger particles have lower thermophoretic velocities. For $\tau^+ = 1.233$, thermophoresis seems to be the only important mechanism, as all particles deposit within a very small range of the corresponding impact velocity. For $\tau^+ = 3.990$, there is another small peak with a higher impact velocity which indicates some deposition by inertia.

These results can be compared with those for DNS without thermophoresis, shown in Fig. 6 using dotted lines. For small particle sizes ($\tau^+ = 0.064$), Brownian diffusion is important as shown by one broad peak. Larger particles (e.g. $\tau^+ = 3.990$) exhibit two peaks: the smaller one corresponding to Brownian deposition and the significantly larger one corresponding to inertial deposition.

Runs 9–11 were done with $u_* = 4\,\mathrm{m\,s^{-1}}$. Temperature fluctuations were turned on for runs 12 and 13. The effect of these on the deposition rate is shown in Fig. 7. Using $u_* = 4\,\mathrm{m\,s^{-1}}$ causes a decrease in the deposition rate, but temperature fluctuations have virtually no effect.

Figures 8 and 9 compare the magnitude of the normal component of the different forces acting on $\tau^+ = 0.064$ and 3.990 particles, respectively. To obtain these values for a given y^+, the numerical channel was divided into 2500 slices in the normal direction. The width of each

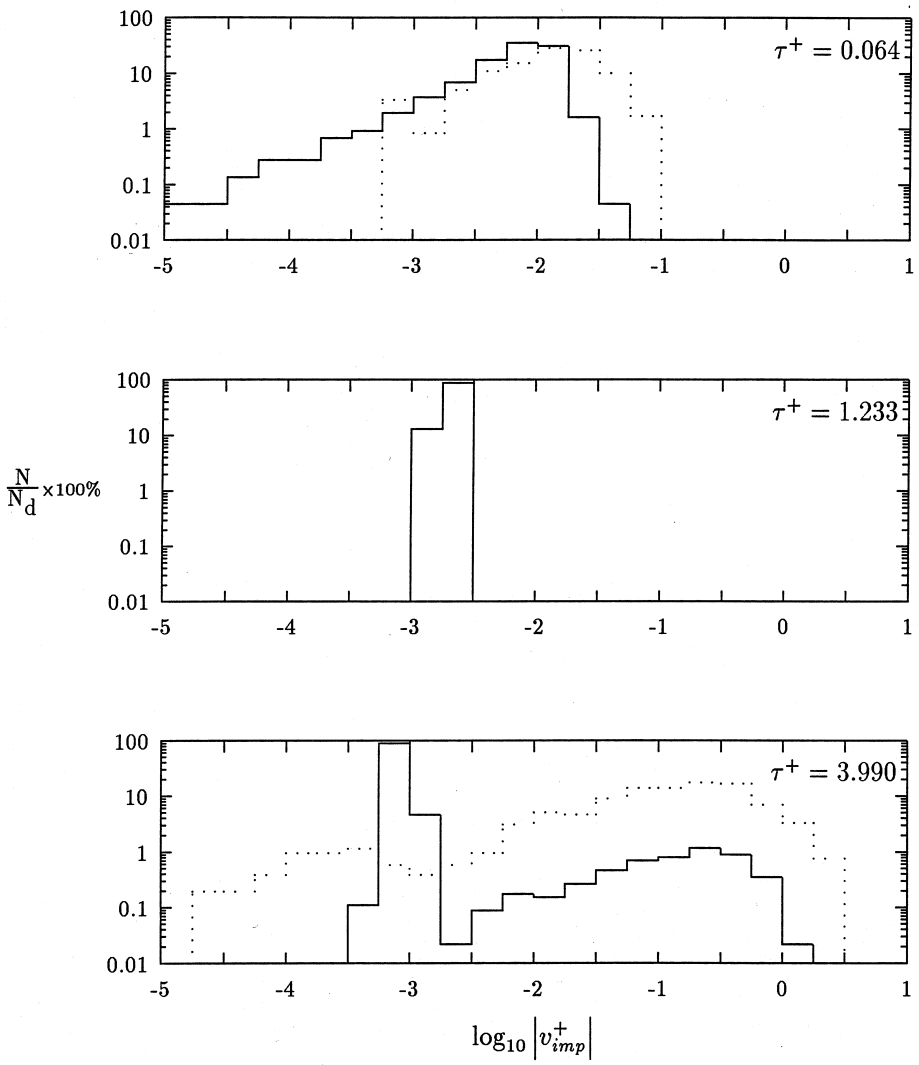

Fig. 6. Impact velocity spectrum for deposited particles for DNS with (—) and without (···) thermophoresis.

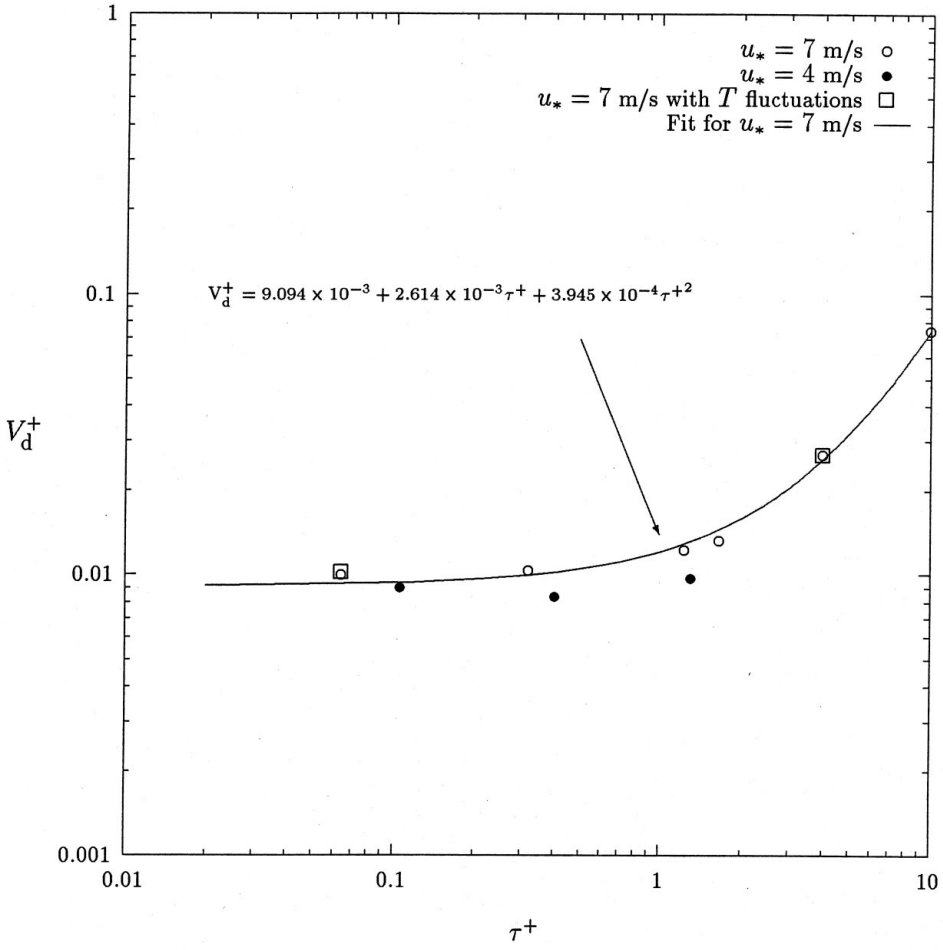

Fig. 7. Effect of temperature fluctuations and u_* on the deposition rate.

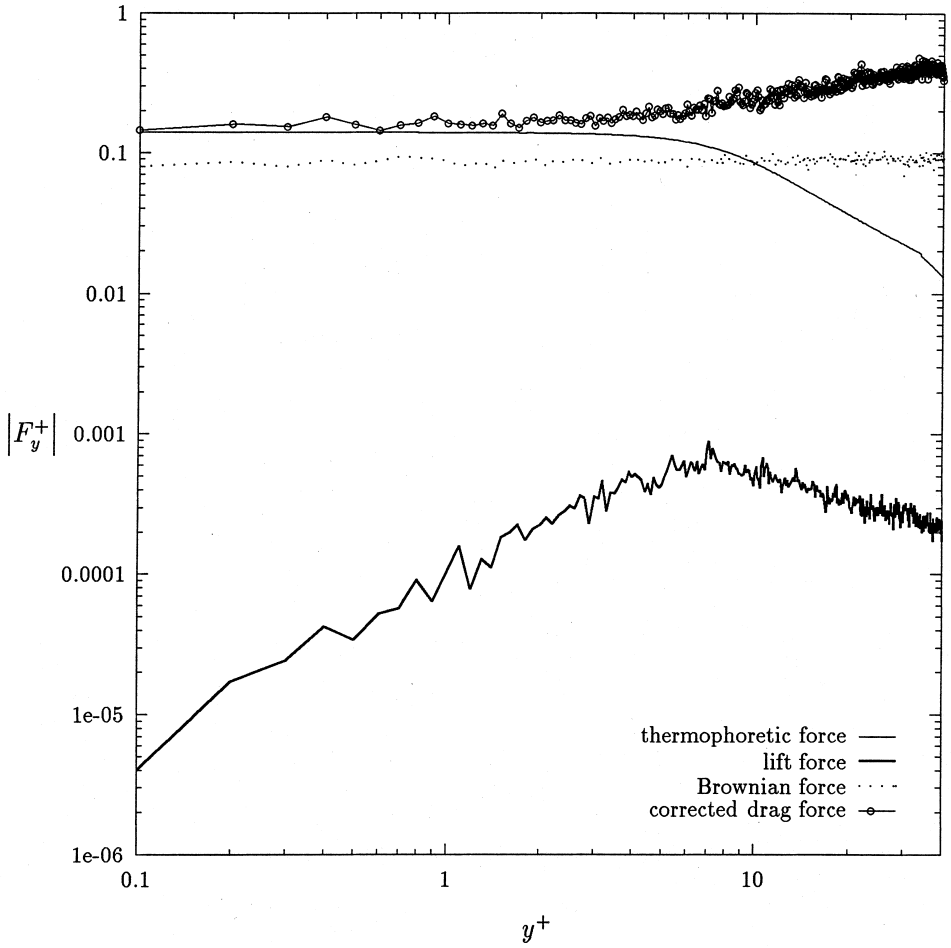

Fig. 8. Comparison of the averaged magnitude of the normal component of different forces acting on $\tau^+ = 0.064$ particles (run 3; averaged over the first 250 time wall units).

slice was 0.1 wall units. The average magnitude of the normal component of the forces were then computed during a DNS run for the particles located in a given slice. The nondimensional gravitational force, which is not plotted, is 1.429×10^{-6} wall units for $u_* = 7\,\mathrm{m\,s^{-1}}$. From the plots, one can see that the magnitude of the dimensionless thermophoretic force experienced by a TiO_2 particle of size 0.05 μm is approximately 100 times larger than that experienced by a particle sized 1.0 μm under the same conditions. Also evident from the figure is the fact that the thermophoretic force is strongest in the region $y^+ < 10$ and then it diminishes rapidly in the core of the channel. This reflects the steep temperature gradient near the wall.

5. Conclusions

DNS results of deposition of TiO_2 particles under the effect of thermophoresis were presented. When compared to DNS without thermophoresis, the deposition rates with thermophoresis show dramatic increases for particles with $\tau^+ = O(1)$. No significant effect due to gravity was found. Turning on the temperature fluctuations also did not produce any change in the deposition rate. Velocity spectrum plots revealed that most of the particles were deposited by thermophoresis.

Acknowledgements

The authors wish to acknowledge the support and facilities of the National Center for Supercomputing Applications at the University of Illinois at Urbana. The authors also acknowledge financial support for this project by DuPont and Clarkson's Center for Advanced Materials Processing (CAMP). This material is based upon work supported in part by the New York State Science and Technology Foundation. Many of the tech-

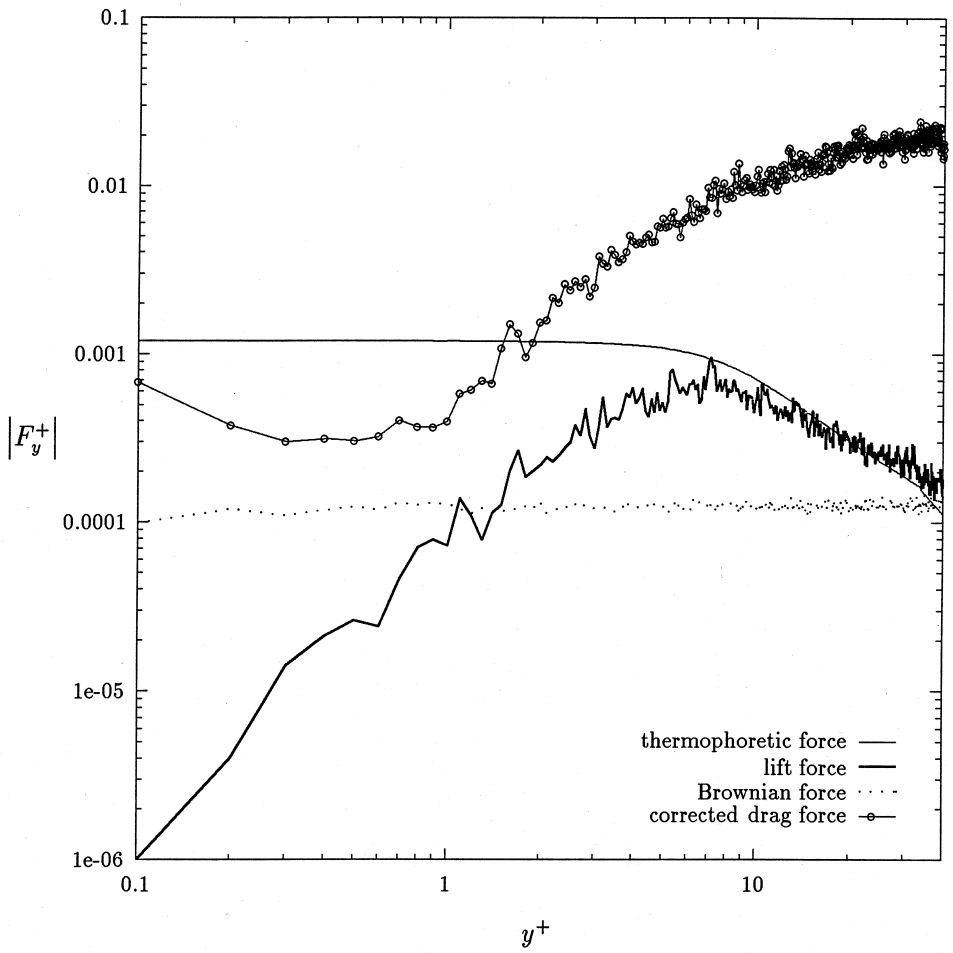

Fig. 9. Comparison of the averaged magnitude of the normal component of different forces acting on $\tau^+ = 3.990$ particles (run 7; averaged over the first 250 time wall units).

niques used in this work were developed with support from Dr Robert Price's program at the United States Department of Energy under contract DE-FG02-88ER13919.

References

[1] Y. Xiong, S.E. Pratsinis, Gas phase production of particles in reactive turbulent flows, Journal of Aerosol Science 22 (1991) 635–655.

[2] B. Derjaguin, Y.I. Rabinovich, A.I. Storozhilova, G.I. Shcherbina, Measurement of the coefficient of thermal slip of gases and the thermophoreses velocity of large-size aerosol particles, Journal of Colloid and Interface Science 57 (1976) 451–461.

[3] K.L. Walker, G.M. Homsy, F.T. Geyling, Thermophoretic deposition of small particles in laminar tube flow, Journal of Colloid and Interface Science 69 (1979) 138–147.

[4] J. Fernandez de la Mora, D.E. Rosner, Effects of inertia of the diffusional deposition of small particles to spheres and cylinders at low Reynolds numbers, Journal of Fluid Mechanics 125 (1982) 379–395.

[5] S.A. Gökoğlu, D.E. Rosner, Correlation of thermophoretically-modified small particle diffusional deposition rates in forced convection systems with variable properties, transpiration cooling, and/or viscous dissipation, International Journal of Heat and Mass Transfer 27 (1984) 639–646.

[6] M. Caporaloni, F. Tampieri, F. Trombetti, O. Vittori, Transfer of particles in nonisotropic air turbulence, Journal of Atmospheric Sciences 32 (1975) 565–568.

[7] M.W. Reeks, The transport of discrete particles in inhomogeneous turbulence, Journal of Aerosol Science 14 (1983) 729–739.

[8] J.B. McLaughlin, Aerosol particle deposition in numerically simulated channel flow, Physics of Fluids A 1 (1989) 1211–1224.

[9] S. Friedlander, H.F. Johnstone, Deposition of suspended particles from turbulent gas streams, Industrial and Engineering Chemistry Fundamentals 49 (1957) 1151–1156.

[10] J.W. Brooke, K. Kontomaris, T.J. Hanaratty, J.B. McLaughlin, Turbulent deposition and trapping of aerosols at a wall, Physics of Fluids A 4 (1992) 825–834.
[11] J.W. Brooke, T.J. Hanratty, J.B. McLaughlin, Free-flight mixing and deposition of aerosols, Physics of Fluids 6 (1994) 3404–3415.
[12] M. Chen, J.B. McLaughlin, A new correlation for the aerosol deposition rate in vertical ducts, Journal of Colloid and Interface Science 169 (1995) 437–455.
[13] R.B. Bird, W.E. Stewart, E.N. Lightfoot, Transport Phenomena, Wiley, New York, 1960, p. 383.
[14] S.L. Lyons, T.J. Hanratty, J.B. McLaughlin, Large-scale computer simulation of fully developed channel flow with heat transfer, International Journal for Numerical Methods in Fluids 13 (1991) 999–1028.
[15] H. Kreplin, H. Eckelmann, Behavior of the three fluctuating velocity components in the wall region of a turbulent channel flow, Physics of Fluids 22 (1979) 1233–1239.
[16] M.A. Niederschulte, Turbulent flow through a rectangular channel, Ph.D. thesis, University of Illinois, Urbana, IL, 1988.
[17] K. Kontomaris, T.J. Hanratty, J.B. McLaughlin, An algorithm for tracking fluid particles in a spectral simulation of turbulent channel flow, Journal of Computational Physics 103 (1992) 231–242.